LETTERS

Migration of the subtropical front as a modulator of glacial climate

Edouard Bard[1] & Rosalind E. M. Rickaby[2]

Ice cores extracted from the Antarctic ice sheet suggest that glacial conditions, and the relationship between isotopically derived temperatures and atmospheric p_{CO_2} have been constant over the last 800,000 years of the Late Pleistocene epoch[1]. But independent lines of evidence, such as the extent of Northern Hemisphere ice sheets[2], sea level[3] and other temperature records[4], point towards a fluctuating severity of glacial periods, particularly during the more extreme glacial stadials centred around 340,000 and 420,000 years ago (marine isotope stages 10 and 12). Previously unidentified mechanisms therefore appear to have mediated the relationship between insolation, CO_2 and climate. Here we test whether northward migration of the subtropical front (STF) off the southeastern coast of South Africa acts as a gatekeeper for the Agulhas current[5,6], which controls the transport of heat and salt from the Indo-Pacific Ocean to the Atlantic Ocean. Using a new 800,000-year record of sea surface temperature and ocean productivity from ocean sediment core MD962077, we demonstrate that during cold stadials (particularly marine isotope stages 10 and 12), productivity peaked and sea surface temperature was up to 6 °C cooler than modern temperatures. This suggests that during these cooler stadials, the STF moved northward by up to 7° latitude, nearly shutting off the Agulhas current. Our results, combined with faunal assemblages from the south Atlantic[7,8] show that variable northwards migration of the Southern Hemisphere STF can modulate the severity of each glacial period by altering the strength of the Agulhas current carrying heat and salt to the Atlantic meridional overturning circulation. We show hence that the degree of northwards migration of the STF can partially decouple global climate from atmospheric partial pressure of carbon dioxide, p_{CO_2}, and help to resolve the long-standing puzzle of differing glacial amplitudes within a consistent range of atmospheric p_{CO_2}.

The fluctuating severity of glacial periods (see Supplementary Information) challenges our understanding of the sensitivity of global climate to forcing by astronomical parameters, and p_{CO_2}. We investigate the migration of the STF in the southern Indian Ocean over multiple glacial cycles to explore whether the latitude of the STF acts as an insolation-sensitive feedback in the climate system, and amplifies low-latitude temperature anomalies to global climate phenomena. The latitude of the STF is determined by the strength and location of atmospheric winds. The subtropical convergence, characterized by negative wind stress curl in the atmosphere and associated Ekman transport convergence in the ocean, denotes the region between the core of the trade winds and the maximum southwesterly winds. Embedded in the subtropical convergence and towards its poleward side is the STF, a zonal band of enhanced productivity and weak (2 °C) meridional sea surface temperature (SST) gradients. The STF defines the southern limit of the subtropical gyres and separates them from the broad eastward flow of the Antarctic circumpolar current (ACC) further south.

We reconstruct the latitude of the STF from hydrographic changes at core MD962077, currently situated under the Agulhas current of the subtropical gyre of the Indian Ocean over the last 800 thousand years (kyr) (see online-only Methods). We test whether northward migration of the STF relative to South Africa acts as a gatekeeper for the leakage of heat and salt between the Atlantic and Indo-Pacific oceans. The Agulhas valve comprises surface and intermediate water transport from the Indian Ocean into the Atlantic. This takes place through the detachment of rings, eddies and filaments from the Agulhas retroflection, consisting of warm and salty Indian Ocean waters and providing a key return route for the supply of waters to the Atlantic meridional overturning circulation (AMOC)[5,6]. Core MD962077 is situated ~7° latitude equatorwards of the modern STF (33.17 °S, 31.25 °E, 3,781 m, Fig. 1), and provides a sensitive monitor of the meridional movements of the STF, which marks the southern boundary of the Agulhas return current.

Our 800-kyr records of SST (U^K_{37}', and $\delta^{18}O$ of *Globigerina inflata* and coccolithophore fraction; Fig. 2a) and biological productivity (abundance of authigenic uranium U_{auth}, total organic carbon TOC and total C_{37} alkenones C_{37tot}; Fig. 2b, data available in Supplementary Information) indicate that each 100-kyr glacial cycle is marked by cooler temperatures and higher productivity, indicating a northerly migration of the STF more proximal to core MD962077, and displaying the same distinctive pattern of a secular trend in the glacial minima. The glacial northward shift of the STF agrees with records from foraminiferal and coccolithophore assemblages in this region[7–11], which highlight that the reappearance and abundance, in the south Atlantic, of the 'Agulhas leakage fauna' is due to a deglacial strengthening of the Agulhas connection.

The marine isotope stages MIS-12 and MIS-10 stand out as exceptionally cool and productive glacial periods. Alkenone-derived SSTs record a subtropical Indian Ocean 4 °C cooler than the Holocene during MIS-2, but MIS-12 and MIS-10 were an additional 2 °C colder. This secular trend in SST is matched by the *G. inflata* $\delta^{18}O$ value (the MIS-12 $\delta^{18}O$ is heavier than that of MIS-2 by 0.5‰, ~2 °C) and coccolithophore fraction $\delta^{18}O$ (MIS-12 is heavier than MIS-2 by 1.5 ‰ but natural effects amplify the coccolithophore fraction $\delta^{18}O$; see online-only Methods). All three productivity proxies imply enhanced productivity during MIS-12 and 10 compared to other glacials. Individually, these proxies cannot be scaled linearly to productivity but are highly sensitive to productivity changes (see online-only Methods). However, the coherence in signal between three SST and productivity proxies, recorded in different phytoplankton and different phases of the sediment susceptible to a range of biases, lends confidence that our secular trend in temperature and productivity is robust.

A picture emerges that the STF migrated northwards towards core MD962077 during each glacial period. During MIS-12 and MIS-10,

[1]CEREGE (UMR 6635), Collège de France, University Paul-Cézanne Aix-Marseille, CNRS, IRD, Europole de l'Arbois BP 80, 13545 Aix-en-Provence Cedex 4, France. [2]Department of Earth Sciences, Oxford University, Parks Road, Oxford OX1 3PR, UK.

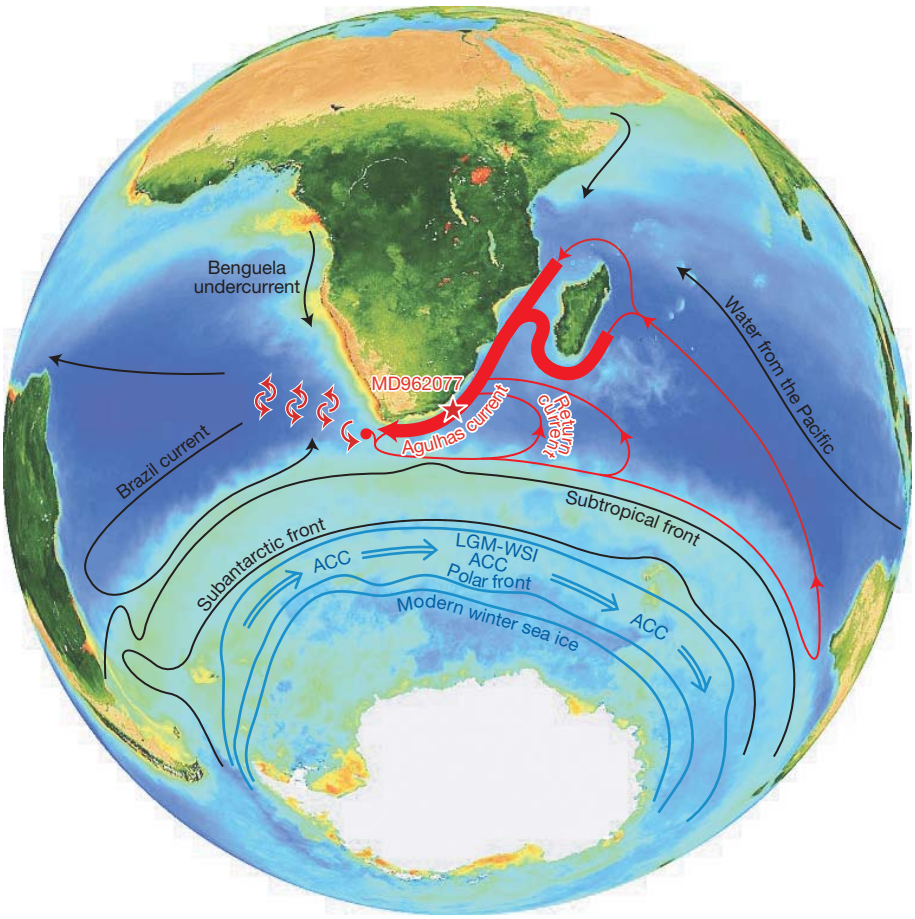

Figure 1 | SeaWiFS (Sea-viewing Wide Field-of-view Sensor) image of ocean colour during austral summer with the highly productive STF to the south of core MD962077 (red star). The core is at present in the path of the Agulhas current, and is influenced by the southward flow of warm and saline waters that are ultimately transported from the Indian to the Atlantic oceans today. The core site is highly sensitive to meridional movements of the fronts in this critical region. LGM-WSI, Last Glacial Maximum winter sea ice extent.

the STF advanced by at least 7° latitude to reach the lowest latitude (33 °S) of the past 800 kyr, as marked by the additional 2 °C cooling that is characteristic of the SST gradient of the modern STF. The STF impinged upon the southern African continent in the Indian Ocean during these extreme glacial periods and almost completely shut down the Agulhas leakage[8,10,11], with a tiny residual, perhaps intermittent, flow to account for the rare occurrence of the Agulhas leakage fauna in cores from the Atlantic sector[11,12]. An associated migration northwards of the southwesterly winds by 5–9° latitude during glacial periods is corroborated by a number of proxy records[13]. This shift and change in intensity of the winds is difficult to capture consistently in intermediate-complexity models[14] and coupled global climate models[15].

We propose that a northerly migration of the STF relative to South Africa acts as a choke point in the climate system. The latitude of the STF has the potential to influence both surface buoyancy fluxes of heat and salt that set the strength and shape of the AMOC[16] and also mixing and wind-driven upwellings that input energy to sustain the AMOC.

As a buoyancy driver of the AMOC, the transport flux of heat and salt in surface waters between the major ocean basins is crucial to return water, salt and heat to the northward flow of the AMOC[17,18]. The exchange of surface water occurs along a 'warm' route and a 'cold' route; the balance between these routes may alter as oceanographic fronts migrate relative to the tips of continents in the Southern Ocean[19]. Important topographic valves restrict the water flow in the Indonesian archipelago, Drake passage, Bering strait and the Agulhas valve of the southern tip of Africa[5]. These valves were drastically different during the 100–150 m sea-level drop of glaciations and could control ocean currents through threshold effects. Our inferred most northerly migration of the STF to 33 °S during MIS-12 and MIS-10 severely reduced the warm saline influence of Indian Ocean thermocline water and the Atlantic salinity budget owing to the Agulhas leakage[5,18–20]. This effect causes cooling and freshening of the Atlantic and implies maximal reduction in North Atlantic deep water formation during MIS-12 and MIS-10.

Energy input to maintain the AMOC derives, in part, from the coupling between strong circumpolar southwesterly winds, which induce a vigorous ACC, upwelling of dense waters from the ocean interior, and northward Ekman transport of waters near the ocean surface[21] as well as southward eddies. Today, the frontal system and associated southwesterly winds cross the continent of South America, which diverts the ACC flow southwards through the Drake passage (56° S). At this point, the ACC is decoupled from the winds and frontal systems that transfer energy to the current[21]. For the rest of the ACC pathway in the modern ocean, the westerly winds align with the ACC. We infer that either the core or meridional extent of the wind field of the southwesterly winds spread to their most northerly position during MIS-12 and MIS-10, and encountered two further continental barriers (Australia at 39 °S, and South Africa at 35 °S), decoupling the topographically constrained ACC to the south from a larger fraction of the frontal-associated winds and reducing the energy transfer to the ocean[21]. These additional circuit breaks in energy transfer from the southwesterly winds to the ACC would amplify a decrease in deep ventilation, on top of a severely reduced Agulhas leakage, during MIS-12 and MIS-10.

To test whether northwards migration of the STF is communicated globally via an influence on AMOC, we consider our data in the context of a record of the $\delta^{13}C$ contrast between deep waters in the

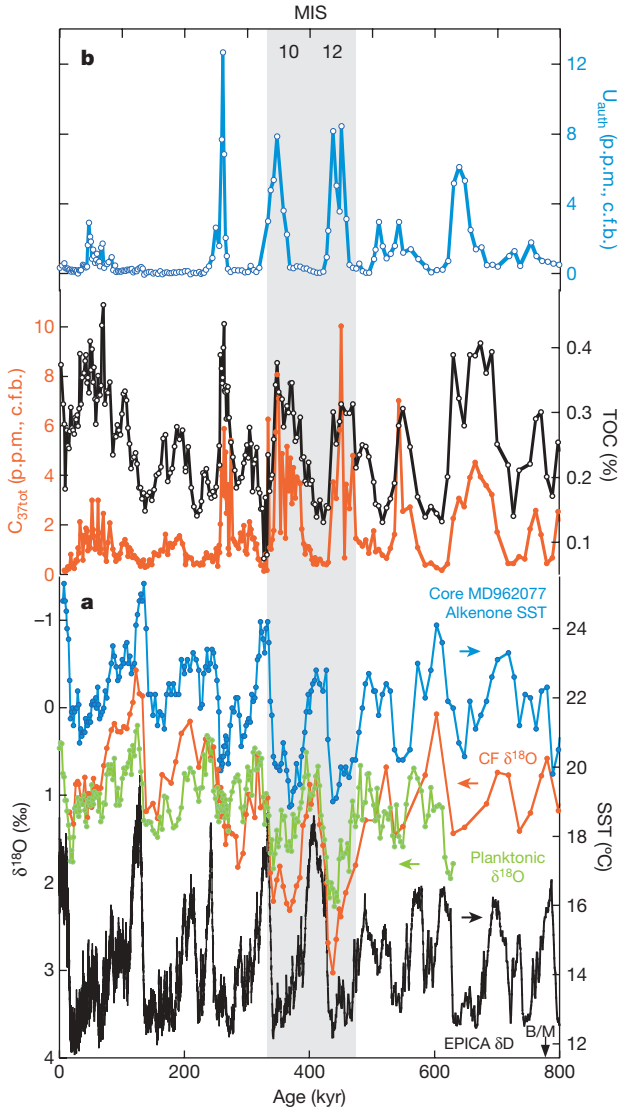

Figure 2 | Long-term trends in SST and productivity-sensitive parameters from core MD962077 compared to the stable baseline glacial temperatures recorded in EPICA Dome C. **a**, Coccolith fraction $\delta^{18}O$ (CF, red dots, left axis), *G. inflata* $\delta^{18}O$ (planktonic, green dots, left axis), and U^{K}_{37}' (alkenone, blue dots, right axis) highlight the evolution of subtropical region glacial SSTs, compared to the stable baseline temperature estimates (black line, the relative abundance of deuterium, δD, scaled according to $(T + 34)/2$ to fit the left axis) from glacial periods in Antarctica recorded in EPICA. The black arrow labelled 'B/M' shows the position of the Brunhes/Matuyama in the deeper section of core MD962077. **b**, Long-term trends of productivity proxies—U_{auth} in parts per million, p.p.m. (blue open circles), percentage TOC (black open circles) and C_{37tot} (red filled circles)—which show high productivity during each glacial period indicative of a northwards migration of the STF. This migration evolves, the STF being at its most northerly position during MIS-12 and MIS-10. (c.f.b., carbonate-free basis; see online-only Methods.)

Atlantic and Pacific oceans, an indicator of the efficiency of deep-ocean ventilation (Fig. 3, Supplementary Information). Our secular trends in temperature and frontal location are accompanied by a glacial decreased contrast between the Pacific and Atlantic deep water masses ($\Delta\delta^{13}C$), with near-zero $\Delta\delta^{13}C$ during MIS-12 and MIS-10; a picture also obtained from the $\delta^{13}C$ vertical gradient in the Southern Ocean[22]. This lack of $\delta^{13}C$ gradient could indicate drastically reduced ventilation of the Atlantic, or enhanced ventilation in the Pacific. Both changes could have occurred with a similar ventilation contribution from the Southern Ocean. Recent numerical simulations of a latitudinal shift of southwesterly winds support a scenario with a decrease of Agulhas leakage by a factor of seven, and a substantial

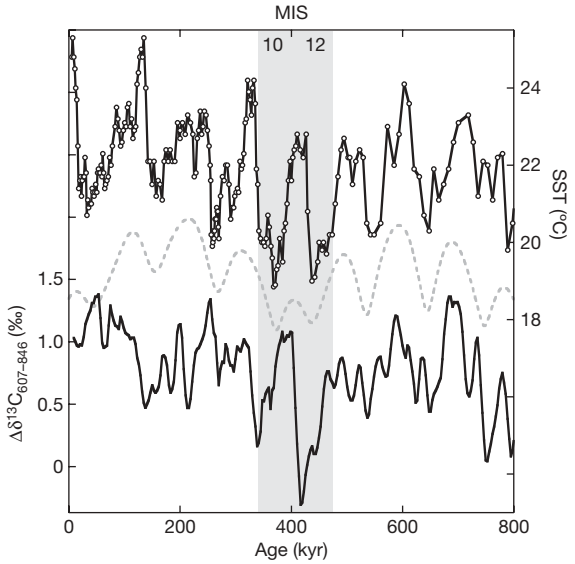

Figure 3 | Mechanistic link between the migration of the STF, orbital eccentricity and ocean overturning. The position of the STF, denoted by our record of SST (black, open circles) co-evolved with orbital eccentricity (grey dashed line) and a measure of overturning strength (black line) based on the $\delta^{13}C$ gradient between the Atlantic (Ocean Drilling Program ODP site 607) and the Pacific (ODP site 846, $\Delta\delta^{13}C$) oceans. This provides an independent measure of the ventilation strength[31] of the AMOC over the last 800 kyr. We derive the $\Delta\delta^{13}C$ value from the difference between the $\delta^{13}C$ values of ODP Site 607 and ODP Site 847.

decrease of North Atlantic deep water transport, with a concomitant increase and deepening of North Pacific convection[20]. These effects result from the wind shift and the enhanced build-up of Pacific surface salinity.

The decrease in ventilation by the AMOC leads to reduced polar heat transport and amplifies the growth of northern ice sheets, and also leads to lowest sea levels during MIS-12 and MIS-10. These frontal choke points of the STF impinging on Australia and South Africa transfer the tropical cooling of MIS-12 and MIS-10 to a global climate signal.

The position of the STF during MIS-12 and 10 could be a response to cooler global climates. Alternatively, a more regional forcing of anomalously cool equatorial temperatures could modulate the position of the STF.

Global cooling drives an equatorward migration of the STF. A global cooling of 3 °C achieves a 7° equatorward migration of the fronts and the peak westerly wind stress position, according to an idealized model[23]. The residual between the EPICA (European Project for Ice-Coring in Antarctica) Dome C temperature record and the temperature component that is linearly linked with greenhouse gas radiative forcing shows a long-term trend of decreasing temperatures towards 400 kyr and increasing towards modern times, in parallel with the longer-term trend of the STF position[24]. However, the minimum levels of p_{CO_2} during MIS-12 and MIS-10 are not exceptionally low compared to other glacial periods[1]. Although increased global coccolithophore production[25] implies a quasi-400-kyr change in the global carbon cycle, Pleistocene trends in p_{CO_2} are compensated biogeochemically[25] or masked by higher-frequency cycles in the record. Exceptional glacial conditions during MIS-12 and MIS-10 require an alternative trigger and amplifier.

Insolation could induce anomalous tropical SSTs that determine the strength of Hadley circulation and position of the STF. Our SST and productivity records show a strong signal at the 100-kyr and 400-kyr frequencies of eccentricity (Fig. 3). Eccentricity modulation of precession may lead to anomalous tropical SSTs owing to a truncated response[26], or to the double maximum of daily irradiation characteristic of the tropics[27,28] rather than the high latitudes.

Forcing at 100-kyr and 400-kyr frequencies is amplified, relative to half-precession, by increasing the fraction of the year over which the maximum and minimum equatorial insolation is time-averaged[28]. Such time-averaging may best approximate the thermal inertia of the tropical SST response to maximum equatorial insolation. Anomalously cool tropical SSTs, caused by low maximum equatorial insolation (modern and about 400 kyr ago), could reduce the Hadley cell (the tropical atmospheric convection cell driven by equatorial heating), draw the STF northwards[28] and act as a trigger for the proposed AMOC positive feedback for exceptional global cooling during MIS-12 and MIS-10.

An implication of the amplification of cooling during MIS-12 and MIS-10 is that there must be some decoupling between Antarctic climate, global climate and p_{CO_2} (ref. 1). The central Antarctic ice sheet may be decoupled from global climatic shifts either by the slow transmission of signals across a strengthened glacial ACC[29] or by the enlarged extent of sea ice during the glacial periods insulating the Antarctic continent from changes in the ocean, analogous to the buffering of Greenland during the extreme cold of Heinrich events by sea ice and the southward migration of the deep ventilation site[30].

It appears that p_{CO_2} can be decoupled from climate at glacial extremes such that insolation modulates the maxima and minima of climate. Modulation of equatorial insolation provides a way of amplifying eccentricity forcing into the climate cycles of Pleistocene glaciations. A proposed mechanism of links between topographic barriers, the STF and the AMOC may explain the puzzling fact that most palaeo-records indicate that glacial periods have different amplitudes. Understanding the effect of the Agulhas valve on ocean circulation is important for modern and future climate studies, as illustrated by recent work on decadal variations of the southwesterly winds[6].

METHODS SUMMARY

The chronology of core MD962077 relies on the last three geomagnetic reversals and tuning of the foraminiferal $\delta^{18}O$ to a global stack. Alkenones were analysed at CEREGE by gas chromatography using an automated Dionex accelerated solvent extractor (ASE-200) to perform lipid extraction. Core MD962077 was sampled every 10–20 cm in plastic vials to measure U, Th and other trace elements by inductively coupled plasma mass spectrometry (ICP-MS). We measured $\delta^{18}O$, in parts per thousand relative to the Vienna Pee Dee Belemnite standard (‰ VPDB) on the multispecies coccolithophore fraction, with minimal contamination from other carbonate components such as foraminiferal fragments. The foraminiferal $\delta^{18}O$ record was previously published[12]. Given the limited constraints on long-term whole-ocean changes in $\delta^{18}O$, and salinity at core MD962077, we have not deconvolved a record of SST from planktonic $\delta^{18}O$. Nonetheless, MIS-12 $\delta^{18}O$ is heavier than MIS-6 by 0.5‰, which is equivalent to a maximum estimate of additional cooling of $\sim$2 °C. The coccolith fraction $\delta^{18}O$ records the largest isotopic change: MIS-12 is heavier than MIS-2 by 1.5‰, but changes in the coccolithophore assemblage occur on these timescales in core MD962077[25] and large interspecific fractionation factors of up to 4‰ can account for a fraction of this change.

Full Methods and any associated references are available in the online version of the paper at www.nature.com/nature.

Received 13 January; accepted 29 May 2009.

1. Luthi, D. *et al.* High-resolution carbon dioxide concentration record 650,000–800,000 years before present. *Nature* **453,** 379–382 (2008).
2. Svendsen, J. I. *et al.* The Quaternary ice sheet history of northern Eurasia. *Quat. Sci. Rev.* **23,** 1229–1271 (2004).
3. Rohling, E. J. *et al.* Magnitude of sea-level lowstands of the past 500,000 years. *Nature* **394,** 162–165 (1998).
4. McManus, J. F. *et al.* A 0.5-million-year record of millennial-scale climate variability in the North Atlantic. *Science* **283,** 971–975 (1999).
5. Lutjeharms, J. R. E. in *The South Atlantic: Present and Past Circulation* (eds Wefer, G., Berger, W. H., Siedler, G. & Webb, D.) 125–162 (Springer, 1996).
6. Biastoch, A., Boning, C. W. & Lutjeharms, J. R. E. Agulhas leakage dynamics affects decadal variability in Atlantic overturning circulation. *Nature* **456,** 489–492 (2008).
7. Flores, J. A., Gersonde, R. & Sierro, F. J. Pleistocene fluctuations in the Agulhas Current Retroflection based on the calcareous plankton record. *Mar. Micropaleontol.* **37,** 1–22 (1999).
8. Peeters, F. J. C. *et al.* Vigorous exchange between the Indian and Atlantic Oceans at the end of the past five glacial periods. *Nature* **430,** 661–665 (2004).
9. Howard, W. R. & Prell, W. L. Late Quaternary Surface circulation of the Southern Indian Ocean and its relationship to orbital variations. *Paleoceanography* **7,** 79–117 (1992).
10. Berger, W. H. & Wefer, G. in *The South Atlantic: Present and Past Circulation* (eds Wefer, G., Berger, W. H., Siedler, G. & Webb, D. J.) 363–410 (Springer, 1996).
11. Bé, A. W. & Duplessy, J. C. Subtropical convergence fluctuations and quaternary climates in the middle latitudes of the Indian Ocean. *Science* **194,** 419–422 (1976).
12. Rau, A., Rogers, J. & Chen, M.-T. Quaternary palaeoceanographic record in giant piston cores off South Africa, possibly include evidence of neotectonism. *Quat. Int.* **148,** 65–77 (2006).
13. Ledru, M. P., Rousseau, D. D., Riccomini, F. W. C. Jr, Karmann, I. & Martin, L. Paleoclimate changes during the last 100,000 yr from a record in the Brazilian Atlantic rainforest region and interhemispheric comparison. *Quat. Res.* **64,** 444–450 (2005).
14. Menviel, L., Timmerman, A., Mouchet, A. & Timm, O. Climate and marine carbon cycle response to changes in the strength of the Southern Hemispheric westerlies. *Paleoceanography* **23,** doi:10.1029/2008PA001604 (2008).
15. Rojas, M. *et al.* The Southern Westerlies during the last glacial maximum in PMIP2 simulations. *Clim. Dyn.*. doi:10.1007/s00382–008–0421–7 (2008).
16. Kuhlbrodt, K. *et al.* On the driving processes of the Atlantic Meridional Overturning Circulation. *Rev. Geophys.* **45,** RG2001 (2004).
17. Gordon, A. L. Interocean exchange of thermocline water. *J. Geophys. Res.* **91,** 5037–5046 (1986).
18. Weijer, W., de Ruijter, W. P. M., Sterl, A. & Drujfhout, S. S. Response of the Atlantic overturning circulation to South Atlantic sources of buoyancy. *Global Planet. Change* **34,** 293–311 (2002).
19. Knorr, G. & Lohmann, G. Southern Ocean origin for the resumption of Atlantic thermohaline circulation during deglaciation. *Nature* **424,** 532–536 (2003).
20. Sijp, W. P. & England, M. H. Southern Hemisphere westerly wind control over the ocean's thermohaline circulation. *J. Clim.*. (in the press).
21. Toggweiler, J. R. & Russell, J. Ocean circulation in a warming climate. *Nature* **451,** 286–288 (2008).
22. Hodell, D. A., Venz, K. A., Charles, C. D. & Ninnemann, U. S. Pleistocene vertical carbon isotope and carbonate gradients in the South Atlantic sector of the Southern Ocean. *Geochem. Geophys. Geosyst.* **4,** doi:10.1029/2002GC000367 (2002).
23. Williams, G. P. & Bryan, K. Ice age winds: an aquaplanet model. *J. Clim.* **19,** 1706–1715 (2006).
24. Masson-Delmotte, V. *et al.* EPICA Dome C record of glacial and interglacial intensities. *Quat. Sci. Rev.* (in the press).
25. Rickaby, R. E. M. *et al.* Coccolith chemistry reveals secular variations in the global ocean carbon cycle? *Earth Planet. Sci. Lett.* **253,** 83–95 (2007).
26. Short, D. A., Mengel, J. G., Crowley, T. J., Hyde, W. T. & North, G. R. Filtering of Milankovitch cycles by Earths geography. *Quat. Res.* **35,** 157–173 (1991).
27. Berger, A., Loutre, M. F. & Melice, J. L. Equatorial insolation: from precession harmonics to eccentricity frequencies. *Clim. Past* **2,** 131–136 (2006).
28. Ashkenazy Y. & Gildor, H. Timing and significance of maximum and minimum equatorial insolation. *Paleoceanography* **23,** PA1206, doi:1029/2007001436 (2008).
29. Schmittner, A., Yoshimori, M. & Weaver, A. J. Instability of glacial climate in a model of the ocean-atmosphere-cryosphere system. *Science* **295,** 1489–1493 (2002).
30. Ganopolski, A. & Rahmstorf, S. Rapid changes of glacial climate simulated in a coupled climate model. *Nature* **409,** 153–158 (2001).
31. Raymo, M. E. *et al.* Stability of North Atlantic water masses in face of pronounced climate variability during the Pleistocene. *Paleoceanography* **19,** PA2008, doi:10.1029/2003PA000921 (2004).

Supplementary Information is linked to the online version of the paper at www.nature.com/nature.

Acknowledgements We thank D. P. Schrag and E. Goddard for their help with analyses in the early stages of this work. We thank C. Sonzogni, F. Rostek, N. Thouveny and J. Carignan for help with analyses and age model, and D. Sansom for help with the figures. We also thank H. Gildor, Y. Ashkenazy, R. Toggweiler, M. Meredith, M.-F. Loutre, P. Huybers and N. Edwards for comments and discussion on an earlier version of this manuscript. R.E.M.R. is grateful to the Royal Society for the International Outgoing Visit award for the exchange visits to CEREGE, which facilitated the development of the ideas and the manuscript. Palaeoclimate work at CEREGE is supported by grants from the Gary Comer Foundation, the CNRS and the Collège de France. Core MD962077 was collected by the RV *Marion Dufresne* supported by the Institut Polaire Français (IPEV).

Author Contributions E.B. and R.E.M.R. contributed equally to this work.

Author Information Reprints and permissions information is available at www.nature.com/reprints. Correspondence and requests for materials should be addressed to E.B. (bard@cerege.fr) or R.E.M.R. (rosr@earth.ox.ac.uk).

METHODS

The chronology of core MD962077 relies on the last three geomagnetic reversals and tuning the foraminiferal $\delta^{18}O$ to the global stack[32]. Alkenones were analysed at CEREGE by gas chromatography following the method of ref. 33 except that an automated Dionex accelerated solvent extractor (ASE-200) was used to perform lipid extraction[34]. Proper identification and quantification of alkenones was verified by gas chromatography mass spectrometry. The analytical precision of the method is about 0.01 units for U^{K}_{37}' (roughly equivalent to 0.3 °C) based on repeated extraction of internal laboratory sediment standard during the course of this study. The accuracy of our procedure has been checked within the framework of the international alkenone intercomparison[35]. For simplicity and to allow comparison with other palaeo-data sets, the SST values were calculated using the equation of ref. 36 which is equivalent to that derived from the core-top compilation[37]. Culture studies show that there is no systematic offset between SST relationships of *Gephyrocapsa oceanica* and *Emiliania huxleyi*[38].

We measured $\delta^{18}O$ on the multispecies coccolithophore fraction, with minimal contamination from other carbonate components such as foraminiferal fragments. The methodology for separating the coccolithophore fraction was based on that of ref. 39. All plasticware was acid-cleaned before use, and deionized water used throughout. 0.5 g of sediment was sieved using 90% proof ethanol through a $<$20 μm sieve. The collected slurry was poured into 15 ml centrifuge tubes and allowed to settle for 10 min. The supernatant containing the suspended particles was pipetted into a second tube and allowed to settle for a further 24 h. The supernatant, considered to contain the major clay fraction, was pipetted away and filtered for recycling. The remaining $<$10 μm fraction was dried and a subsample taken and rinsed three times with deionized water to ensure elimination of any relict ethanol. A small fraction was weighed into boats for analysis by stable isotope mass spectrometry (PRISM at Harvard University). The foraminiferal $\delta^{18}O$ record was previously published[12]: for each analysis, 60 specimens of *Globorotalia inflata* were picked from the 250–350 μm fraction and analysed at the National Taiwan Ocean University in Keelung using standard procedures. Given the limited constraints on long-term whole-ocean changes in $\delta^{18}O$, and salinity at core MD962077, we have not deconvolved a record of SST from planktonic $\delta^{18}O$. Nonetheless, MIS-12 $\delta^{18}O$ is heavier than MIS-6 by 0.5‰, equivalent to a maximum estimate of additional cooling of ~2 °C. The coccolith fraction $\delta^{18}O$ records the largest isotopic change: MIS-12 is heavier than MIS-2 by 1.5‰, but changes in the coccolithophore assemblage occur on these timescales in this core[25] and large interspecific fractionation factors of up to 4‰ can account for a fraction of this change[40]. Measuring three thermometric proxies such as U^{K}_{37}' of alkenones and $\delta^{18}O$ of both foraminifera and coccoliths is important because these independent proxies provide confirmation of temperature trends. Indeed, it is crucial to be able to rule out possible artefacts related to species, seasonality or habitat depth of signal markers and of post-deposition processes such as sediment mixing. Differential smoothing or lagging can occur in sediments between different size fractions of the same core[41]. In core MD962077, the $\delta^{18}O$ of coccoliths is measured in the same fine fraction as alkenones, while the $\delta^{18}O$ of foraminifera belong to the coarse fraction. When similar trends are observed for the three proxies (as is the case), it is possible to rule out such an artefact as an alternative explanation to temperature changes.

Core MD962077 was sampled every 10–20 cm in plastic vials to measure U, Th and other trace elements by ICP-MS. Procedures are similar to those used in our previous work[42] except that ICP-MS measurements were performed with a Perkin-Elmer Elan 6000 at Service d'Analyse des Roches et des Mineraux (SARM) of the CNRS in Nancy, France. For both elements, the uncertainty is $<$5% and the determination level is 0.01 p.p.m. U_{auth} concentrations were calculated by subtracting a crustal component determined from the measured Th concentration and a detrital Th/U weight ratio of 4.71 (ref. 43). The detrital U correction is relatively small (about 1 p.p.m. on average) in comparison with the observed U variations. Moreover, U and U_{auth} profiles are roughly parallel and the two records exhibit the same variability. Therefore, using either the U or U_{auth} profile would not change the interpretation of our results. All concentrations shown in Fig. 2b were converted to concentrations on a carbonate-free basis (c.f.b.), which is the conventional procedure to account for the effect of dilution by carbonate (see ref. 42 for example). The U_{auth}, TOC and C_{37tot} concentration profiles with and without this correction are roughly parallel and using raw concentrations would lead to the same interpretation.

TOC, C_{37tot} and U_{auth} concentrations have been used as proxies for the biological productivity in the Southern Ocean related to migrations of the STF and the subantarctic front[44,45]. Following the work of these authors and from our own studies in other regions[42,46] it is clear that these proxies cannot be scaled linearly to productivity. Indeed, the organic carbon raining from the surface is partly remineralized in the sediments, which creates more-reducing conditions, leading to U diffusion in pore waters and trapping in the sediments[44]. These reducing conditions also lead to preferential preservation of lipids such as alkenones, which always exhibit a much larger dynamic range than observed with TOC[46]. Trace metals can also be remobilized by additional processes such as oxic front diffusion and bioturbation[47]. All these natural processes are superimposed on each other, making these markers only qualitative, although very sensitive, proxies for the surface productivity. Despite these complications, the strength of our approach is that we consider all three proxies measured independently. When TOC, C_{37tot} and U_{auth} trends agree, indicating enhanced values, it is reasonable to assume that the observed maxima are associated with a significant productivity increase linked to the STF migration. MIS-12 and MIS-10 are indeed characterized by maxima of TOC, C_{37tot} and U_{auth}.

32. Lisiecki, L. E. & Raymo, M. E. A Pliocene-Pleistocene stack of 57 globally distributed benthic $\delta^{18}O$ records. *Paleoceanography* **20**, PA1003 (2005).
33. Sonzogni, C. *et al.* Core-top calibration of the alkenone index vs sea surface temperature in the Indian Ocean. *Deep-Sea Res.* **44**, 1445–1460 (1997).
34. Pailler, D. & Bard, E. High frequency paleoceanographic changes during the past 140,000 years recorded by the organic matter in sediments off the Iberian Margin. *Palaeogeogr. Palaeoclim. Palaeoecol.* **181**, 431–452 (2002).
35. Rosell-Melé, A. *et al.* Precision of the current methods to measure the alkenone proxy UK37′ and absolute abundance in sediments: results of an interlaboratory comparison study. *Geochem. Geophys. Geosyst.* **2**, 2000GC000141, 1–28 (2001).
36. Prahl, F. G., Muehlhausen, L. A. & Zahnle, D. L. Further evaluation of long-chain alkenones as indicators of paleoceanographic conditions. *Geochim. Cosmochim. Acta* **52**, 2303–2310 (1988).
37. Müller, P. J., Kirst, G., Ruhland, G., von Storch, I. & Rosell-Mele, A. Calibration of the alkenone paleotemperature index U^{k}_{37}' based on core-tops from the eastern South Atlantic and the global ocean (60°N–60°S). *Geochim. Cosmochim. Acta* **62**, 1757–1772 (1998).
38. Conte, M., Thompson, A., Lesley, D. & Harris, R. P. Genetic and physiological influences on the alkenone/alkenoate versus growth temperature relationship in *Emiliania huxleyi* and *Gephyrocapsa oceanica*. *Geochim. Cosmochim. Acta* **62**, 51–68 (1998).
39. Stoll, H. M. & Schrag, D. P. Coccolith Sr/Ca as a new indicator of coccolithophorid calcification and growth rate. *Geochem. Geophys. Geosyst.* **1**, doi:10.1029/1999GC000015 (2000).
40. Ziveri, P. *et al.* Stable isotope ''vital effects'' in coccolith calcite. *Earth Planet. Sci. Lett.* **210**, 137–149 (2003).
41. Bard, E. Paleoceanographic implications of the difference in deep-sea sediment mixing between large and fine particles. *Paleoceanography* **16**, 235–239 (2001).
42. Pailler, D. *et al.* Burial of redox-sensitive metals and organic matter in the equatorial Indian Ocean linked to precession. *Geochim. Cosmochim. Acta* **66**, 849–865 (2002).
43. Taylor, S. R. & McLennan, S. M. *The Continental Crust: Its Composition and Evolution* (Blackwell, 1985).
44. Rosenthal, Y., Boyle, E. A., Labeyrie, L. & Oppo, D. Glacial enrichments of authigenic Cd and U in subantarctic sediments—a climatic control on the element's oceanic budget. *Paleoceanography* **10**, 395–413 (1995).
45. Sachs, J. P. & Anderson, R. F. Increased productivity in the Subantarctic ocean during Heinrich events. *Nature* **434**, 1118–1121 (2005).
46. Schulte, S. & Bard, E. Past changes in biologically mediated dissolution of calcite above the chemical lysocline recorded in Indian ocean sediments. *Quat. Sci. Rev.* **22**, 1757–1770 (2003).
47. Zheng, Y., Anderson, R. F., Van Geen, A. & Fleisher, M. Q. Remobilization of authigenic uranium in marine sediments by bioturbation. *Geochim. Cosmochim. Acta* **66**, 1759–1772 (2002).

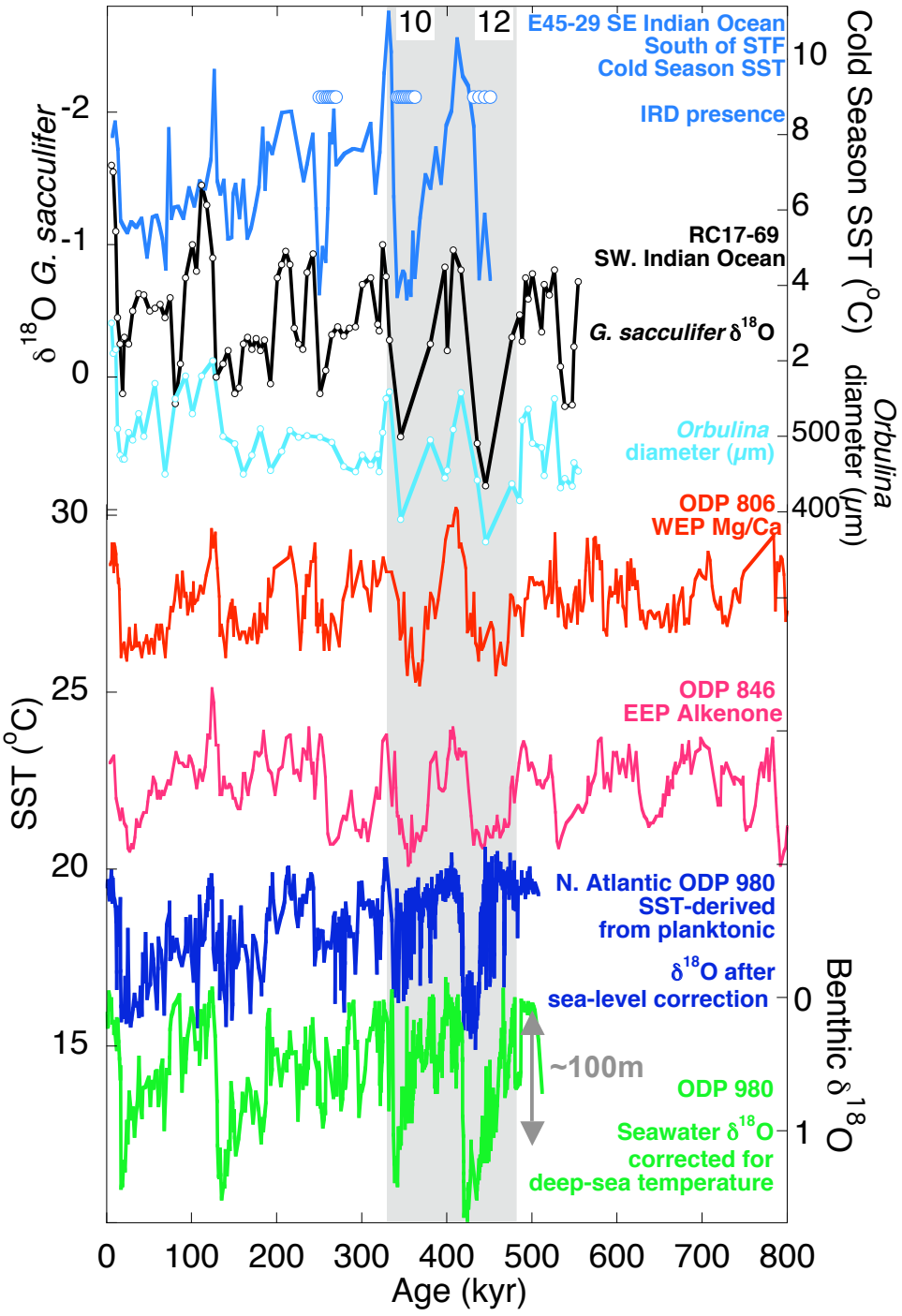

Fig. S1. Long-term evolution of SSTs in marine sites from the global ocean, compared to a sea-level curve (the grey arrow indicates ~100m of sealevel change). The sea-level curve is derived from benthic $\delta^{18}O$ in the ODP Site 980 from the North Atlantic and

corrected for a 3ºC glacial-interglacial temperature change[4] (green). Across the zonal gradient of the equatorial Pacific, Mg/Ca in the West Equatorial Pacific warm pool[48,49] (red) and U^{K}_{37}' estimates in the upwelling waters of the eastern Equatorial Pacific[50] (pink) show an additional cooling of 0.5-1 °C during MIS-12 and 10 compared to other glacial stages. In the subtropical Indian Ocean, our new U^{K}_{37}' SST record shows an additional cooling of 2 ºC (Fig. 2a). This observation is consistent with records of $\delta^{18}O$ in *Globigerina sacculifer* (black) and the temperature sensitive *Orbulina* diameter (turquoise) from RC17-69 in the SE Indian Ocean[11]; and with the exceptional northwards migration of the Polar front during MIS-12 and 10 derived from cold season SST estimates, and the presence of ice rafted debris (IRD) at core E45-29 situated between the present day STF and the Polar Front in the SW Indian Ocean[9] (blue). A 1°C additional cooling is also identified in the high latitude North Atlantic summer SST record (dark blue)[4], obtained by correcting the $\delta^{18}O$ of *Neogloboquadrina pachyderma (d)* from its ice volume component using the benthic $\delta^{18}O$ signal (scaled to fit axes according to the equation (8 + (derived SST)/2)).

Supplementary Notes

1. Variable severity between glacials

Many paleoclimate reconstructions show that the glacial periods of the Late Quaternary were not of equivalent severity. In his seminal 1987 paper, Shackleton[51] listed MIS-12 as an "exceptionally large glaciation", with ice volume ~ 15% greater that the last glacial maximum (MIS-2). Shackleton also concluded that MIS 12 likely corresponds to the extensive Elsterian glaciation identified from glacial geology of northern Europe (Anglian of the British Isles). More recently, several other benthic

$\delta^{18}O$ records from single cores[e.g.4] and from global compilations[32] support the view that MIS-12 was more extreme than the LGM and other glacial maxima. The quantitative interpretation of benthic and planktonic $\delta^{18}O$ records is notoriously difficult because the sea level component is mixed with those linked to calcification temperature (and local salinity for planktonic records). Nevertheless, $\delta^{18}O$ records corrected for temperature effects do confirm the exceptional conditions that prevailed during MIS-12 (see Fig. 3 in ref. 4).

The ultimate way to reconstruct the global sea level during MIS-12 and 10 would be to drill, and date by U-series, corals or submerged speleothems corresponding these sea level low-stands. Recent studies reported new important data on MIS-6 and 8 [52-54], but sampling glacial maxima older than the LGM is still a long-term but challenging goal. Fortunately, glacial low stands can be studied in particular archives such as sediments from the Red Sea[3] and submerged shorelines from the Gulf of Lion in front of the Rhone Delta[55]. The identification of MIS-12 is based on the continuity of sediment sequences (in deep-sea cores or high-resolution seismic stratigraphy). These independent sea level reconstructions confirm the variable altitude of glacial low-stands. In particular, sea levels during MIS-12 and 10 were about 150 m below modern, lower by ~ 20%, than during MIS-2.

In addition to these sea level data, there is multiple evidence from regional glacial geology to indicate that MIS-2 did not correspond to the maximum extent of continental ice sheets during the Quaternary (see two recent studies for a comprehensive view of the Fennoscandian Ice sheet[2] and for mapping of the glacial moraines of the southern margin of Laurentide ice sheet[56]). A similar conclusion was reached by Hughes et al.[57] based on moraines of mountain glaciers from Greece. U-Th

ages of carbonates in tills allowed these authors to conclude that MIS-12 was the most extensive glaciation recorded in the Mediterranean region, a view supported by long pollen time series such as those from Tenaghi-Philippon and Ioannina[58].

The catastrophic opening of the English Channel was recently attributed to the overflow of a large pro-glacial lake formed in front of an enormous ice sheet complex merging the Fennoscandian and British ice domes[59]. This event is dated to the Elsterian-Anglian stage, the equivalent of MIS-12. It appears from other terrestrial paleo-data in Europe and North America that MIS-12 (Elsterian-Anglian in Northern Europe, and Kansan in North America) corresponds to the most extreme glaciation of the Late Pleistocene[51,60]. As stressed by Kukla and Cilek[60] "several of the cold climate episodes recorded on land appear more severe than the remainder". MIS-12 is a case of extreme climate change as shown by records from Southern to Central Europe and the East Asian monsoon area[61].

A range of measures of past sea surface temperature (SST), also reveal thermal contrasts between different glacial periods of the late Pleistocene across the global surface ocean[4,48-50]. These ~0.5-1 Myr temperature records highlight MIS-12 and 10 as glacial periods of exceptional surface cooling (Fig. S1). In the subantarctic Southern Ocean, summer SSTs dip unusually during MIS-12 to those characteristic of the Polar Front and are accompanied by the largest ice rafted detritus (IRD) peak of the Pleistocene record[62]. Indeed, the frontal systems in the southern hemisphere of the Indian and Pacific Oceans show exceptional northwards migration during MIS-12 and 10[9,63]. Besides low SST, the exceptional nature of MIS-12 in the North Atlantic is marked by enhanced millennial scale variability compared to all other glacial periods[4,64].

2. $\delta^{13}C$ as a ventilation proxy.

We use the difference in benthic $\delta^{13}C$ between the Atlantic and the Pacific as a measure of ventilation strength. The characteristic signature of deepwater masses is dictated by the $\delta^{13}C$ of the surface waters in the source area of that deepwater mass. This surface signature in part reflects the nutrient content: $\delta^{13}C$ mirrors nutrients due to the preferential uptake of ^{12}C during photosynthesis; and in part reflects the air-sea equilibrium between atmospheric CO_2, and the ocean dissolved inorganic carbon[65]. The signature of deepwater $\delta^{13}C$, which is preserved in benthic foraminifera at any core site, is dictated by the degree of mixing of these isotopically distinct deepwater masses and their ventilation "age" or overprint by the regenerative flux of isotopically light carbon from decaying organic matter raining from the surface ocean. For this reason, there are clear correlations between $\delta^{13}C$, the Apparent Oxygen Utilization (AOU) and the radiocarbon ages of deep water masses of the world ocean[66].

In order to assess the degree of overturning of the global ocean throughout the last 800 kyrs, we have calculated the gradient or difference in $\delta^{13}C$ between the Atlantic (ODP site 607) and Pacific (ODP Site 846) from the original $\delta^{13}C$ benthic records[67-69] ($\Delta\delta^{13}C$). In the modern ocean, nutrient depleted and isotopically heavy (positive $\delta^{13}C$) northern sourced deepwaters are thought to be transported from the Atlantic via the Antarctic Circumpolar Current, where mixing takes places with nutrient replete and isotopically light (negative $\delta^{13}C$) southern sourced water, to the Pacific. This transport results in a gradient from relatively positive $\delta^{13}C$ values in the Atlantic to lighter $\delta^{13}C$ values in the Pacific due to mixing and "aging". By contrast, during MIS-10 and MIS-12, this gradient between the ocean basins ceases to exist. Such a lack of $\delta^{13}C$ gradient implies that both ocean basins are seeing either the same water mass or different water masses

but of similar ventilation age. In each case, the implication is a drastically reduced ventilation of the Atlantic, or enhanced ventilation in the Pacific as simulated with numerical models[20].

Supplementary References

48. Medina-Elizalde, M., & Lea D. W., The Mid-Pleistocene Transition in the Tropical Pacific, *Science,* **310,** 1009-1012, (2005)

49. Lea, D. W., D. K. Pak, & Spero, H. J. Climate impact of late Quaternary equatorial Pacific sea surface temperature variations. *Science* **289**, 1719-1724. (2000).

50. Liu, Z. H. and T. D. Herbert High-latitude influence on the eastern equatorial Pacific climate in the early Pleistocene epoch. *Nature* **427**, 720-723 (2004).

51. Shackleton N.J., Oxygen isotopes, ice volume and sea level. *Quat. Sci. Rev.* **6,** 183-190, (1987).

52. Dutton A., Bard E., Antonioli F., Esat T.M., Lambeck K., McCulloch M.T., Phasing and amplitude of sea level and climate change during the penultimate interglacial. *Nature Geosci.* **4,** DOI :10.1038/NGEO470, (2009).

53. Camoin, G. F., Ebren, P., Eisenhauer, A., Bard, E., & Faure, G., A 300,000-yr coral reef record of sea level changes, Mururoa atoll (Tuamotu

archipelago, French Polynesia, *Paleogeogr. Paleaoclimatol. Paleoecol.,* **175,** 325-341 (2001)

54. Thomas, A. L., Henderson, G. M., Deschamps, P., Yokoyama, Y., Mason, A. J., Bard, E., Hamelin, B., Durand, N., Camoin, G. Sea-level timing across the penultimate deglaciation: U/Th dating of corals from Tahiti. *Science* **324,** 1186-1189 (2009).

55. Rabineau, M, Berné, S., Olivet, J.-L., Aslanian, D., Guillocheau, F., Joseph, P. Paleo sea levels reconsidered from direct observation of paleoshoreline position during Glacial Maxima for the last 500,000 yr. *Earth Planet. Sci. Letts.* **252,** 119-137 (2006).

56. INQUA Commission on Glaciation, Pre-Wisconsin Glaciation of Central North America. Work Group on Geospatial Analysis of Glaciated Environments (GAGE), Emporia State University, Emporia, Kansas (2000).

57. Hughes, P.D., Woodward, J.C. & Gibbard, P.L. Middle Pleistocene cold stage climates in the Mediterranean: new evidence from the glacial record. *Earth Planet. Sci. Letts.* **253,** 50-56 (2007)

58. Tzedakis, P. C., McManus, J. F., Hooghiemstra, H., Oppo, D. W., & Wijmstra, T. A. Comparison of changes in vegetation in northeast Greece with records of climate variability on orbital and suborbital frequencies over the last 450 000 years. *Earth Planet. Sci. Letts* **212**, 197-212 (2003).

59. Gupta, S., Collier, J. S., Palmer-Felgate, A., & Potter, G., Catastropic flooding origin of shelf valley systems in the English Channel. *Nature* **448,** 342-345 (2007).

60. Kukla, G. & Cilek V., Plio-pleistocene megacycles: Record of climate and tectonics. *Palaeogeogr. Palaeoclimatol. Palaeoecol.* **120**, 171-194 (1996).

61. Rousseau, D., Wu, N., Pei Y., & Li, F. Three exceptionally strong East-Asian summer monsoon events during glacial conditions in the past 470 kyrs, *Climate of the Past Discussions* **4,** 1289-1317 (2008)

62. Becquey, S. & Gersonde, R. Past hydrographic and climatic changes in the Subantarctic Zone of the South Atlantic - The Pleistocene record from ODP Site 1090, *Palaeogeog., Palaeoclimatol., Palaeoecol.*, **182,** 221-239 (2002)

63. Schaefer G., Rodger, J. S., Hayward, B. W., Kennett, J. P., Sabaab, A. T., & Scott, G. H. Planktic foraminiferal and sea surface temperature record during the last 1 Myr across the Subtropical Front, Southwest Pacific, *Mar. Micropaleo.,* **54,** 191-212 (2005)

64. Billups, K., Lindley, C., Fisler, J., & Martin, P. Mid Pleistocene climate instability in the subtropical northwestern Atlantic, *Glob. Planet. Change.* **54,** 251-262 (2006).

65. Lynch-Stieglitz, J., Stocker, T. F., Broecker, W. S., & Fairbanks, R. G. The influence of air-sea exchange on the isotopic composition of oceanic carbon: Observations and modelling*, Glob. Biogeochem. Cycles.,* **9,** 653-665 (1995)

66. Broecker W. S., & Peng, T. H., Tracers in the sea : Eldigio Press Lamont Doherty Geological Observatory, 1982, 690 pages (1982)

67. Ruddiman, W.F., Raymo, M.E., Martinson, D.G., Clement, B.M. & Backman, J., Mid-Pleistocene evolution of Northern Hemisphere climate, *Paleoceanogr.,* **4,** 353-412 (1989).

68. Raymo, M.E., Ruddiman, W.F., Backman J., Clement, B.M. & Martinson, D.G. Late Pliocene variation in Northern Hemisphere ice sheets and North Atlantic deep water circulation, *Paleoceanogr.,* **4,** 413-446 (1989).

69. Mix, A.C., Le, J., & Shackleton, N. J., Benthic foraminiferal stable isotope stratigraphy of Site 846; 0-1.8 Ma, *Proceed. Ocean Drill. Prog., Sci. Res.,* **138,** 839-854 (1995).